

# Droplet-Based Sensing: Optical Microresonator Sensors Embedded in Digital Electrowetting Microfluidics Systems

Matthew White Royal, Nan M. Jokerst, *Fellow, IEEE*, and Richard B. Fair, *Fellow, IEEE*

**Abstract**—Electrowetting-on-dielectric (EWD) microfluidics is an emerging platform for practical applications such as water quality testing and medical diagnostics. Low power consumption, low sample and reagent volumes, small size, and rapid fluid transport are features of electrowetting microfluidic platforms that will enable the development of cost-effective, rapid time-to-result, and portable point-of-care diagnostic devices. Microresonator sensors are an excellent sensor technology for integration into these microfluidic systems, because they perform high sensitivity detection of proteins, DNA, and other biologically relevant molecules while tolerating a droplet oil encapsulation layer. This paper reports on a SU-8 polymer microresonator embedded in the top plate of the EWD system, which enables addressing of the sensor with a single droplet of <100 nL in volume and enables droplets to be moved onto and off of the sensor. This system is the first to demonstrate analyte measurement by electrowetting actuation of droplets onto and off of a top plate integrated microresonator sensor. Both photolithographically patterned and electron beam lithographically patterned microresonator sensors were tested, and the effect of a conventional filler medium, silicone oil, on the sensor sensitivity was investigated.

**Index Terms**—Electrowetting, microresonator, sensor, integrated POC devices.

## I. INTRODUCTION

**P**ORTABLE, point-of-care (POC) clinical diagnostics are emerging for diagnosing diseases that require complex assays, such as those utilizing DNA identification, for applications ranging from treating diseases in the developing world to personalized healthcare [1]. POC diagnostic systems optimally have attributes that include low cost, low power consumption, small size, low reagent consumption, high accuracy, rapid time-to-result, and ruggedness [1]. Several components are necessary in such a system, including a sensor to detect biomolecular targets, a microfluidic system to perform sample preparation, interface/control electronics, and packaging [1]. These POC systems prepare samples for the sensor, performing operations that include extracting and processing

target molecules, such as DNA or proteins, from complex samples such as blood, and actuating the sample to the sensor. The sensor function is to detect the target molecules with high sensitivity, low limit of detection, high speed, and low power consumption in a compact package.

A wide variety of microfluidic platforms [1], [2] and sensor technologies [3]–[5] have been developed to address the needs of sample preparation and analyte detection, respectively. One of the major challenges in the realization of a POC system capable of handling complex immunoassays is the integration of sensors into microfluidic systems, such that both the microfluidic system and the sensor maintain the desired attributes for a POC device. This paper reports on the integration of a microresonator optical sensor directly into the top plate of a digital electrowetting-on-dielectric (EWD) microfluidic system, and explores the design, optimization, and test of these integrated systems. The results presented herein demonstrate, for the first time, that such an integrated EWD system can perform all standard EWD functions, including moving droplets onto and off of the sensor in the integrated system, and sense the target analyte.

Microfluidic platforms can be categorized as continuous flow microfluidics and droplet-based microfluidics [2]–[6]. Pressure driven continuous flow microfluidic systems are used extensively in laboratories and have been implemented in some commercial devices [1], because they are both inexpensive and easy to fabricate. However, pressure driven systems typically require external pumps that consume a relatively large amount of power and contain a large amount of ‘dead volume’, which is fluid that performs no other useful function other than to facilitate fluid flow [1]. Droplet-based microfluidic systems, in which fluids are driven in the form of discrete droplets, have much less dead volume than continuous flow systems, which results in reduced reagent usage and more efficient use of limited sample material. Droplet-based systems can perform complex assays involving sample preparation from complex samples, but with very low power and without pumps [7], [8]. Thus, droplet-based systems address the need for low power, low reagent consumption, and small size in POC systems.

There are six major types of droplet-based microfluidic actuation technologies, including segmented flow, surface acoustic wave, dielectrophoresis, magnetic, and electrowetting-on-dielectric (EWD) [2], [9]. Segmented flow devices are pressure driven and use power hungry active pumps. Dielectrophoresis is very similar to EWD for the actuation of liquid droplets,

Manuscript received June 24, 2012; accepted July 8, 2013. Date of publication July 23, 2013; date of current version October 4, 2013. This work was supported by the National Science Foundation under Grant CNS-1135853. The work of M. W. Royal was supported by the Air Force Office of Scientific Research through a National Defense Science and Engineering Graduate Fellowship. The associate editor coordinating the review of this paper and approving it for publication was Dr. Richard T. Kouzes.

The authors are with the Electrical and Computer Engineering Department, Duke University, Durham, NC 27708 USA (e-mail: mwr9@duke.edu; nan.jokerst@duke.edu; rfair@ee.duke.edu).

Color versions of one or more of the figures in this paper are available online at <http://ieeexplore.ieee.org>.

Digital Object Identifier 10.1109/JSEN.2013.2273828

but is more limited than EWD in terms of actuation speed and fluid compatibility [9], [10]. Magnetic actuation typically requires droplets to contain magnetic beads, which limits flexibility [11]. Surface acoustic wave (SAW) devices can actuate droplets of fluid regardless of polarizability or ion content [2]. However, the power required to transport droplets is high (watts to milliwatts of power) [12]–[14]. EWD, while more sensitive to fluid properties than SAW, is capable of actuating most biologically relevant fluids [15] and can manipulate droplets containing as little as a few tens of picoliters of fluid [16] with power consumption in the microwatts to nanowatts range [17]. Additionally, EWD can perform sample preparation functions using magnetic bead based methods, including extraction and amplification of DNA with the polymerase chain reaction (PCR) [7], [8].

An important aspect of droplet-based flow systems is the need for a particular immiscible gas or liquid medium to surround the droplets of fluid to facilitate functionality of the flow device. For systems with enclosed flow channels, liquid media are most commonly used, and include silicone oil, dodecane, and hexadecane [18]. The medium performs functions that include preventing evaporation and surface fouling [2], [17]. The silicone oil in EWD also reduces the actuation voltage required to move the droplets, increasing the device reliability and reducing power consumption [17].

The performance of any sensor integrated with an EWD system should be evaluated in the presence of the immiscible liquid. Many highly sensitive biosensors transduce a signal produced by a change in a material property on or near the surface of the sensor (surface sensing), which include electrical [4], mechanical [5], and optical [3] sensors. Some examples of these types of sensors include microcantilevers [19], surface plasmon resonance (SPR) sensors [20], optical microresonators [21], [22], electrochemical impedance spectroscopy sensors [23], and ion sensitive field effect transistors (ISFETs) [24]. Surface sensing sensors are highly sensitive, with a low limit of detection (LOD - detecting single molecules [25], [26]). Many of these sensors are also planar devices, which can be fabricated with low cost, well-established fabrication technologies that leverage Si manufacturing [27]. Surface sensors are also capable of label-free detection, and elimination of labels translates to reduced reagent costs.

Optical waveguide sensors, of which microresonator sensors and SPR sensors are two examples, are uniquely suited for sensing in the presence of an oil medium. Optical waveguide sensors can be utilized to sense changes in the refractive index several hundred nanometers from the surface [28] and thus, through a thin film of oil. Microresonators are of particular interest, because they are among the most compact of optical sensors, which enables high density integration of sensor arrays [29], and because they can be fabricated with low cost polymer materials [21], [30]–[32]. Thus, the focus of this work is the integration of a planar, polymer optical microresonator sensor into the top plate of an EWD system, and to explore the design and optimization of the system, while evaluating the effect of the liquid immiscible medium on the performance of the microresonator sensor.

Microresonator sensors have been utilized to detect biologically relevant analytes, such as proteins and DNA [29], [30], [33]. Microresonator sensors detect these analytes by responding to small changes in refractive index near the surface of the resonator. The guided optical mode in the microresonator waveguide has an evanescent tail that extends outside of the wall of the microresonator cavity, which enables the guided mode to interact with the material outside of the cavity. When the refractive index of the region interacting with the evanescent tail changes, the phase velocity, or the effective refractive index of the guided mode changes slightly. The resonant cavity converts this change in effective refractive index to a change in the resonant wavelength, which can be observed as a shift in the spectral features corresponding to the resonant wavelengths in the microresonator spectrum. The ability of a microresonator sensor, as well as optical waveguide-based sensors in general, to respond to changes in refractive index at a significant distance from the waveguide structure makes them uniquely suitable for application in droplet-based microfluidics systems that utilize a liquid immiscible medium. The evanescent tail of the guided mode can penetrate through a thin film of the immiscible liquid medium that exists between the droplet and the waveguide. Thus, material can be sensed by an optical microresonator sensor in a droplet, despite the presence of a liquid immiscible medium between the droplet and the sensor, such as silicone oil [34], [35].

The performance of a microresonator sensor is described by several factors. The smallest change in refractive index that can be detected by measuring a shift in the microresonator resonance wavelength is the limit of detection (LOD), which is inversely proportional to the product of the quality factor ( $Q$ ), defined by the sharpness of the resonances, and the sensitivity ( $S$ ), defined by the response slope [36], [37]. The product of  $Q$  and  $S$  is the figure-of-merit (FOM). The  $Q$  factor is primarily affected by bending loss, surface scattering loss, material absorption, and waveguide coupling loss [38], [39]. Decreasing these losses increases (optimizes) the  $Q$  factor. The microresonator sensitivity is defined as the ratio of the shift in the resonant wavelength to the change in refractive index in the target material surrounding the microresonator and is usually given in units of nm/RIU (RIU = refractive index unit). Sensitivity is affected by the cross-sectional dimensions of the microresonator waveguide and the refractive indices of the materials comprising the waveguide [40]–[42]. A higher refractive index waveguide core material, holding the refractive indices of the surrounding materials constant, generally results in a higher maximum sensor sensitivity [42].

There are a number of microresonator geometries that could potentially be integrated with an EWD system. Microresonator sensors have been demonstrated in a variety of geometries, including three-dimensional spheres [43] and toroids [44], and two-dimensional planar shapes [30], [31], [45]. Three-dimensional microresonator structures, while having the highest  $Q$  factors, are not optimal for low cost planar fabrication processes [27]. Planar microresonators are better suited for low cost fabrication and microfluidics integration. Planar microresonator sensors consist of ring [30], disk [31], spiral-shaped

(or folded cavity) [45], and slot-waveguide [41] structures in either organic (polymer) or inorganic materials. The ring geometry is preferable among the planar geometries, because it is the most compact geometry and it can be designed to support a single guided mode, regardless of the bend radius.

Materials for microresonators fall into two classes, inorganics and organics (e.g. polymers). Inorganic materials have high refractive indices ( $n > 1.6$ ) [46], which enables small size (small bending radius) and high sensitivity [42], [47]. To realize high sensitivity microresonators with inorganic materials, high resolution optical lithography or electron beam lithography is required, because the device dimensions are too small for standard photolithography [47]. The relatively low refractive index of polymers enables high performance microresonator sensors using low cost photolithography [21], [30]–[32], which motivates the integration of polymer microresonators with EWD systems towards the development of a POC system. Conventional polymer materials for optical applications have a lower refractive index ( $n < 1.6$ ) than most inorganic materials [46]. Thus, a challenge with polymer microresonator sensors is to achieve high performance, or, given the specific application, an appropriate level of performance.

Previous work on SU-8 polymer optical microresonators bonded on top of an EWD system demonstrated that the microresonator would function in the presence of an immiscible oil medium [34], [35]. However, that system addressed the sensor through a hole in the top plate of the EWD system and did not preserve the EWD functionality; droplets could not be moved off of the sensor. The system described herein fully supports the microfluidic system functionality by embedding the microresonator sensor and associated bus waveguides into the EWD system top plate. In the previously reported system, a large quantity of liquid had to be dispensed onto the sensor in order to make contact with the sensor through the hole in the top plate. By embedding the sensor in the top plate, the sensor was addressable by a single droplet and the ability to move droplets onto and off of the sensor was demonstrated. To assess the performance of the sensor integrated with the EWD system, glucose sensing was performed both by merging glucose containing droplets with a droplet in contact with a sensor (droplet merging), and by replacing the droplet in contact with the sensor with a glucose containing droplet (droplet swapping). Sensor sensitivity was assessed in silicone oil of two different viscosities, 20 cSt and 2 cSt, and was compared to the sensitivity measured without silicone oil.

To investigate the performance of SU-8 microresonators, both photolithographically (PL) patterned and electron-beam lithographically (EBL) patterned sensors were fabricated and tested. The performance of the PL sensors matched that of the EWD integrated microresonator sensors reported previously. In parallel with the development of the integrated EWD system, the sensitivity and loss as a function of the microresonator waveguide width and height were investigated theoretically and experimentally, using EBL to masklessly (quickly) vary the patterned devices. The EBL patterned sensors had

significantly improved FOMs compared to the PL patterned sensors, demonstrating that high performance microresonators can be integrated with an EWD system that is fully functional.

## II. INTEGRATED MICRORESONATOR SENSOR-ELECTROWETTING MICROFLUIDIC SYSTEM DESIGN AND FABRICATION

### A. Design

The EWD embedded microresonator system combines two independent systems, the EWD microfluidic system and the optical sensing system, which includes the microresonator sensor and its bus waveguides, into an intimately integrated single system. Some aspects of the two systems were designed independently, whereas other aspects were co-designed. The following discussion explores the design aspects of each system and the rationale behind the design choices.

1) *Microresonator Design Considerations:* Microresonator sensors detect small changes in refractive index near the surface of the resonator, which result in a shift in the resonant wavelengths of the cavity. The spectral features corresponding to the microresonator resonant wavelengths appear as peaks in the drop port of the optical system and as nulls in the throughput port of the optical system, as depicted in Fig. 1(a). Light is coupled into and out of the cavity using bus waveguides adjacent to the microresonator and the spectrum can be read out from either or both of the bus waveguide exit ports.

For the embedded microresonator structure, a vertical coupling configuration was utilized in which the bus waveguides were vertically separated from the microresonator by an interlayer dielectric. Vertical coupling of the microresonator has advantages compared to lateral coupling (where the bus waveguides are horizontally separated from the resonator), including precise control of the coupling between the bus waveguides and the microresonator, due to precise control of the interlayer dielectric thickness through deposition [48], insensitivity of the coupling efficiency to small misalignments [48], reduced surface scattering loss and input/output coupling loss to the bus waveguides [48], isolation of the coupling regions from analytes [21], and isolation of the bus waveguides from the microfluidics gasket materials. Additionally, there are advantages associated with vertical coupling that are particular to integration with EWD microfluidics, including reduced optical absorption in the bus waveguides from the top plate conductive ground plane layer and reduced non-uniformity in the fluoropolymer layer and the conductive ground plane layer thicknesses, due to mitigation of step coverage effects.

For the vertical coupling geometry, the interlayer dielectric thickness can be adjusted, such that the insertion loss (the optical loss from input to output) at the drop port and the Q factor are well balanced, resulting in a higher FOM. Decoupling the microresonator from the bus waveguides by increasing the thickness of the interlayer dielectric between them increases the microresonator Q factor at the cost of increased insertion loss, or reduced transmission, at the drop port [32], [38]. The boundary condition used herein was to maintain transmission on resonance (transmission at a peak

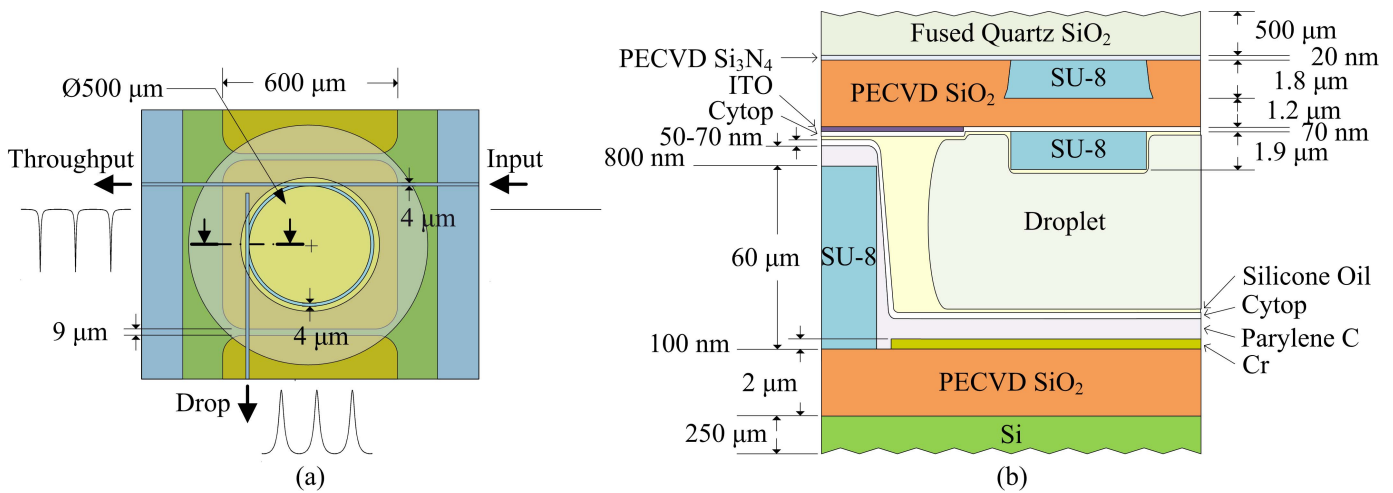


Fig. 1. Diagram of the integrated sensor structure. (a) Top view (not to scale). The optical spectrum at each bus waveguide port is depicted by the small figures adjacent to the ports. (b) Side view (not to scale).

wavelength) at the drop port above  $-50$  dBm, which could be detected with the lightwave test equipment. Microresonator devices were fabricated on Si for FOM optimization, and on glass for EWD integration. Typically, the top plate embedded sensor optical transmission was 5–15 dB lower than that of the test devices fabricated on Si. The reduced coupling efficiency was attributed to the lower waveguide facet quality on the glass substrates (which were diced) as compared to the Si substrates (which were cleaved) and to the absorption from the conductive ground plane in the EWD integrated system. The interlayer dielectric that balanced transmission at the drop port with Q factor for the PL patterned sensors was  $1.2 \mu\text{m}$ . The microresonator waveguides for the PL patterned sensors were  $4 \mu\text{m}$  wide and  $\sim 1.9 \mu\text{m}$  high. The bus waveguide width and height were  $4 \mu\text{m}$  and  $1.8 \mu\text{m}$ , respectively. For the EBL patterned sensors, the interlayer dielectric thickness was  $1.4 \mu\text{m}$ , the microresonator waveguide widths were  $1.2 \mu\text{m}$  and  $1.5 \mu\text{m}$  (to increase the sensitivity), and the bus waveguide dimensions were reduced to  $850 \text{ nm}$  in height and about  $1.7 \mu\text{m}$  in width to better phase match with the smaller microresonator waveguide. A top view of the integrated system is shown in Fig. 1(a) and a side view showing the cross section of both the bottom plate and the microresonator embedded in the top plate is shown in Fig. 1(b).

**2) EWD Design Considerations:** In EWD, droplets are actuated by applying a voltage to the electrowetting electrodes. The electric field modulates the surface tension of the droplet, which moves the droplet to the electrode with the applied voltage. By applying voltages to a time series of electrodes, droplets can be moved through the system, according to the layout of the electrodes.

A typical EWD device consists of a bottom plate and a top plate sandwiching a gasket that encloses the fluid reservoirs and flow channels. The bottom plate contains the electrowetting electrodes coated with a dielectric film and a hydrophobic layer (a fluoropolymer, e.g. Teflon or Cytop), and the gasket. The top plate contains a conductive ground plane coated with a hydrophobic material with no

patterned components, which makes it a good location to embed sensors.

The EWD microfluidic bottom plate studied herein consisted of four reservoirs with large electrodes connected by a series of smaller, closely spaced electrodes. These electrowetting electrodes were individually connected to larger control pads for connection to external contact pins. The small electrowetting electrodes had a pitch of  $605 \mu\text{m}$  and the gasket height was about one-tenth of that value ( $\sim 60 \mu\text{m}$ ). This ratio was chosen to minimize the droplet dispensing and splitting voltage [16]. Fig. 1(a) and Fig. 1(b) show the top and side views, respectively, of the EWD structure with the relevant dimensional parameters. Multiple reservoirs were included to enable different liquids to be supplied to the system, as well as a waste reservoir to sequester used fluids. Thirty two electrodes were used in the design, and the full system layout is shown in Fig. 2.

**3) EWD-Microresonator Co-Design Considerations:** The insertion loss of the optical system is affected by propagation loss in the bus waveguides, which is proportional to the length of the bus waveguides, as well as coupling loss from coupling with the microresonator. Insertion loss is important for both the power efficiency of the optical system as well as for the LOD, because the magnitude of the signal relative to the intensity noise affects the accuracy of the resonant wavelength estimation [37]. The bus waveguides had an estimated propagation loss of  $\sim 7 \text{ dB/cm}$ , so the path length was minimized to reduce insertion loss. The propagation length from input to output was  $2.2\text{--}2.5 \text{ cm}$  (the path lengths were slightly different for light exiting the drop and the throughput ports). The electrowetting electrode pitch was set to  $605 \mu\text{m}$  to ensure that the EWD device size would be small enough to fit on a 2" wafer and match the droplet size to the microresonator. The droplet diameter is roughly that of the diagonal of the electrodes, so the size of the electrodes limit the diameter of the microring resonator sensor. The diameter of the microresonator was set to  $500 \mu\text{m}$  to fit within the area of one electrowetting electrode with some alignment tolerance. This diameter is in the range

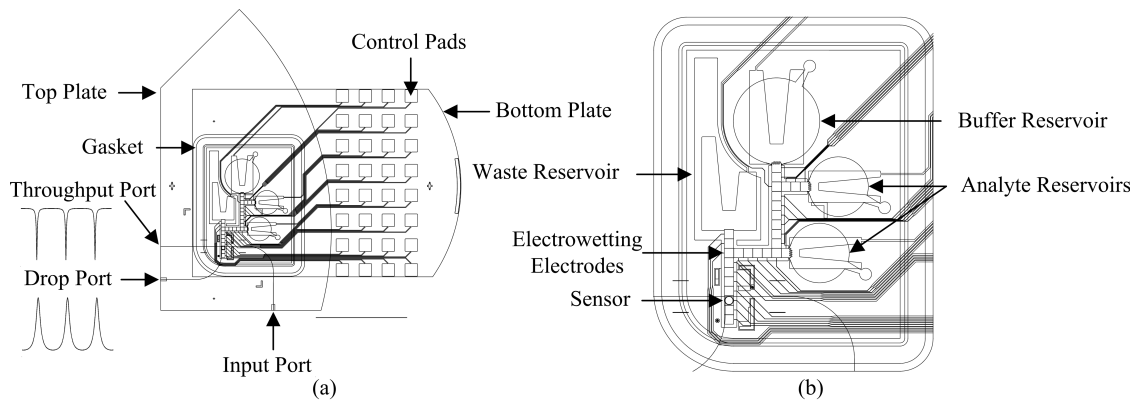


Fig. 2. Scaled CAD drawings of the EWD embedded microresonator system. (a) Full system. The optical spectrum at each bus waveguide port in log scale is illustrated by the small figures adjacent to the ports. (b) Close-up of the gasket.

where larger diameter microresonators significantly increase the FOM by reducing the bending loss, which drove the decision to use resonators of this size.

The microresonator sensor was integrated into the EWD system top plate, which necessitated some modifications to the standard top plate design. To integrate a sensor into the top plate, generally both the fluoropolymer and the transparent conductive film on the top plate would need to be patterned in order not to interfere with the sensor functionality. This patterning would adversely affect the movement of droplets onto and off of the sensor. One design innovation was to pattern the microresonator ring on top of the fluoropolymer film. This was accomplished by reversibly modulating the hydrophobicity of the fluoropolymer film by treatment with oxygen plasma to render the surface hydrophilic prior to coating with the SU-8 polymer film (for SU-8 adhesion) and subsequent high temperature baking to restore the hydrophobicity after patterning the microresonator [49], [50]. The ground plane transparent conductor (ITO) absorbs near the operational wavelength of 1550 nm, because this wavelength is close to its plasma frequency [51], resulting in optical losses. To address this problem, a region of the ITO, 550  $\mu\text{m}$  in diameter and centered on the 500  $\mu\text{m}$  diameter sensor location, was removed by wet etching to avoid losses, but was left intact elsewhere.

The optical coupling from the bus waveguides into the gasket material was studied, because this coupling was expected to introduce additional optical loss. The material layers of the bottom plate (Fig. 1) included SU-8 3000 ( $n \sim 1.555$ ) [52], Parylene C ( $n \sim 1.639$ ) [53], and Cytop ( $n \sim 1.34$ ) [54]. Because the refractive index of the parylene was higher than the SU-8 2002 ( $n \sim 1.569$ ) [55] used to make the bus waveguides, optical loss due to coupling from the bus waveguides into the gasket was possible. However, the interlayer dielectric was sufficiently thick to block the gasket coupling. No significant change in propagation loss was experimentally observed in the bus waveguides with and without the gasket in contact with the top plate. Thinner interlayer dielectric layers could result in gasket coupling losses.

## B. Fabrication

1) *Microresonator*: For the PL patterned microresonators, the top plate was fabricated on one quarter of a 4", 500  $\mu\text{m}$  thick fused quartz wafer. A 20 nm etch stop layer of PECVD SiN was deposited, followed by a 2  $\mu\text{m}$  thick layer of PECVD SiO<sub>2</sub>. A Cr etch mask was then evaporated and patterned using photoresist, and 1020 Cr etchant was used to etch the Cr. Reactive ion etching (RIE) was used to etch trenches into the PECVD SiO<sub>2</sub>, followed by a short etch in buffered oxide etchant (BOE). After the BOE etch, the Cr etch mask was removed, and the trenches were filled with spin coated SU-8 2002 polymer. After a soft cure, the SU-8 was exposed and hard cured. The SU-8 film was next etched down to the trench with RIE, and then 1.2  $\mu\text{m}$  of PECVD SiO<sub>2</sub> was deposited on top of the channel waveguides. Indium-tin oxide (ITO, 70 nm) was sputter deposited onto the PECVD SiO<sub>2</sub>, and the ITO was patterned by using photoresist and etching with a 5% HCl solution. The glass substrate was diced using a scribe & break tool to expose the waveguide facets. A hydrophobic layer of Cytop about 50–70 nm thick was spin-coated on top of the ITO and cured. The surface was exposed to oxygen plasma to render the Cytop surface hydrophilic. To form the microresonator, SU-8 2002 was spin coated, soft cured, exposed, developed, and hard cured.

For the EBL patterned microresonators, the fabrication process was similar, but with the photolithography steps replaced with electron beam lithography steps. More detailed process information can be found in [56].

2) *EWD Microfluidics*: The bottom plate was fabricated on a 2" Si wafer by first coating the wafer with 2  $\mu\text{m}$  of SiO<sub>2</sub> by PECVD. The Cr electrodes were patterned using photolithography and wet etching, following a standard EWD fabrication process [57]. To form the gasket, SU-8 3035 was spun on, patterned, developed, and hard cured. Approximately 800 nm of Parylene C was vacuum deposited, followed by a hydrophobic coating of  $\sim 50$ –70 nm of spin coated Cytop. The system was assembled by aligning the top plate to the bottom plate gasket and mechanically compressing the two plates together.

### III. TEST AND MEASUREMENT

#### A. Measurements

The optical spectral measurements were first conducted on non-integrated sensor test structures, followed by the integrated system. These measurements utilized an HP8164A Lightwave Measurement System with an 81680A tunable laser module, an 81623A Ge photodetector module, and an 81618A optical head interface module. The HP8164A was controlled with Labview. A Corning SMF 28 single-mode fiber was used to launch light into the input waveguide and a Corning 62.5/125  $\mu\text{m}$  multimode, graded-index fiber was used to collect light from the output waveguides. For the non-integrated sensor characterization, a step size of 0.6 pm over a small range of wavelengths within the mode-hop free range of the laser, 1520 nm–1570 nm, was used. A step size of 0.6 pm balanced temporal and wavelength resolution, because smaller step sizes required lower wavelength sweep rates. For the non-integrated sensor sensitivity measurements, a range of wavelengths encompassing three resonances was utilized for a spectral measurement rate of 1 every 6 seconds, on average. For measurements in the integrated system, the maximum wavelength sweep range was utilized, which resulted in about one measurement every 12 seconds. For each condition of the sensor, immersion in DI H<sub>2</sub>O or immersion in D-glucose solution, about 30 spectral measurements were made. Resonant wavelength shifts in time were limited to no greater than one-half of the free spectral range (FSR, the spacing between the resonant peaks) from one spectral measurement to the next, to ensure that large shifts between spectral measurements, which would preclude tracking of the resonances, would not occur. Thus, spectral measurements were taken as frequently as possible and the refractive index shifts were controlled by appropriately diluting the target analyte.

#### B. Data Analysis

Resonant wavelength traces, or sensorgrams, which show the resonant wavelength versus time, were calculated from the measured spectra for each experiment. First, spectra were filtered with a zero phase low-pass filter to remove high frequency intensity noise. After filtering, the resonant wavelengths were estimated from the local maxima appearing in the spectra. After identifying all of the resonant wavelengths in each spectral measurement, the resonances were tracked in time by applying a time domain filter, which tracked each peak from one frame to the next by assuming that the peak located in each frame was associated with the nearest peak in the previous frame, under the constraint that each estimated peak location could not shift from its previous position more than one half of the microresonator FSR from one frame to the next. The result of applying this analysis to the measured spectral data was a series of sensorgrams corresponding to each peak appearing in the spectra. Analysis of the sensorgram was used to estimate the resonant wavelength shift caused by a change in glucose concentration.

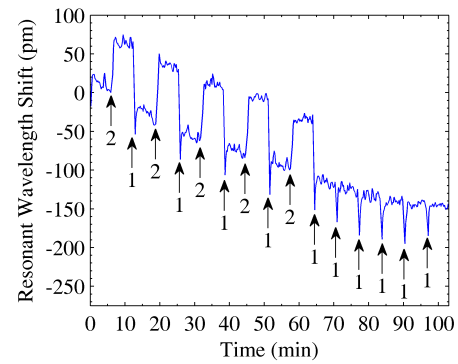


Fig. 3. Resonant wavelength trace showing 5 replicates of swapping a DI H<sub>2</sub>O droplet with a 2% glucose droplet, followed by 5 replicates of swapping a DI H<sub>2</sub>O droplet with a DI H<sub>2</sub>O droplet. The device under test was a PL patterned top plate-embedded microresonator. 1- Droplet swapped with a 20  $\mu\text{L}$  DI H<sub>2</sub>O droplet. 2- Droplet swapped with a 20  $\mu\text{L}$  2% D-glucose droplet.

#### C. Sensor Performance Characterization

To compare the nominal sensor sensitivity, which is the sensitivity measured in an air medium, to the sensor sensitivity when measured in a silicone oil medium, the sensitivity was measured both outside of the microfluidics system without the presence of oil and inside of the microfluidics system with silicone oil, using D-glucose solution as a refractive index reference. D-glucose solution has a refractive index dependence on concentration of  $1.4 \times 10^{-3}$  RIU/%(w/w) [58]. To estimate the sensor sensitivity without the EWD system, a droplet of deionized (DI) water was swapped with 2% D-glucose solution on the sensor by alternately removing the initial droplet with a gentle spray of N<sub>2</sub> and quickly pipetting the next droplet of solution onto the sensor.

The droplet swapping technique involved first applying a 20  $\mu\text{L}$  droplet of de-ionized (DI) water to the sensor. Next, the droplet was removed with a gentle spray of high purity N<sub>2</sub> gas and quickly replaced with either a 20  $\mu\text{L}$  droplet of 2% D-glucose or a 20  $\mu\text{L}$  droplet of DI water. Swapping of DI water with 2% D-glucose and with DI water was repeated five times to obtain a good estimate of the sensitivity of the sensor to glucose and of the baseline noise caused by the swapping operation. Fig. 3 shows the results of the droplet swapping measurement for a PL patterned microresonator sensor that was integrated into an EWD top plate, but measured external to the EWD system. The sensitivity of the PL patterned sensor was calculated by estimating the wavelength shifts from the wavelength trace shown in Fig. 3. Baseline drift, which was attributed to the water absorption known to occur with SU-8 polymer [59], was subtracted from the data prior to estimating the shift. The mean wavelength shift for the five glucose measurements was about 73 pm and the standard deviation was about 8.7 pm. The baseline shifts due to swapping water droplets were less than 2 pm and comparable to the resonant wavelength measurement noise. Using the estimated refractive index of the glucose solution, the sensitivity was estimated to be 26 nm/RIU.

For the EBL patterned sensors, the sensitivity was measured using the same method [56]. An EBL patterned test sensor

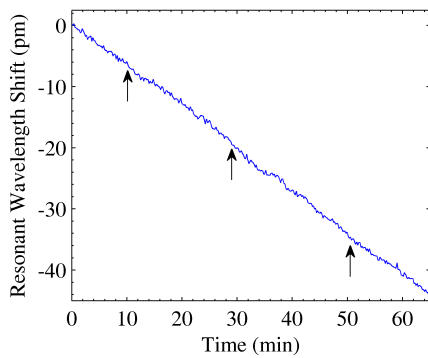


Fig. 4. Resonant wavelength trace showing droplet merging in the electrowetting system. Droplet merging times are indicated by the arrows.

fabricated on an  $\text{SiO}_2/\text{Si}$  substrate with a microresonator waveguide width of  $1.5 \mu\text{m}$  had a measured sensitivity of  $82 \text{ nm/RIU}$ . An EBL patterned top plate embedded sensor with a microresonator waveguide width of  $1.2 \mu\text{m}$  had a measured sensitivity of  $89 \text{ nm/RIU}$  and the guided mode polarization for that device was identified as transverse magnetic (TM). Thus, reducing the microresonator waveguide width significantly increased the sensitivity.

To determine the Q factor and FOM of the sensors, their spectra were measured from the drop port with the sensor immersed in water. The Q factor of the PL sensor, the ratio of the resonance peak wavelength to the full width of the peak at half maximum, was 24,000 in water, yielding a FOM of  $0.62 \times 10^6 \text{ nm/RIU}$ . Q factors for the EBL patterned sensors were 15,000 and 8,400 for the test sensor and the top plate embedded sensor, respectively. FOMs for the EBL patterned sensors were  $1.2 \times 10^6 \text{ nm/RIU}$  and  $0.76 \times 10^6 \text{ nm/RIU}$  for the test sensor and the top plate embedded sensor, respectively. Thus, the performance of the EBL patterned sensors was generally improved relative to the PL patterned sensors by a significant increase in sensitivity at the cost of a reduced Q factor. The FOM for the EBL test sensor was comparable to that of other polymer microresonators, including those made with polystyrene ( $1 \times 10^6 \text{ nm/RIU}$  at  $1550 \text{ nm}$ ) [30], SU-8 ( $2.3 \times 10^6 \text{ nm/RIU}$  at  $1310 \text{ nm}$ ) [32], and ZPU13-430/LFR-S708U ( $2 \times 10^6 \text{ nm/RIU}$  at  $1550 \text{ nm}$ ) [21].

#### D. EWD Integrated Sensor Performance Characterization

##### 1) Droplet Merging:

a) *Baseline Test:* Merging operations, and the effect of these operations on the sensor measurements, were evaluated in the integrated microresonator/EWD system by merging several DI water droplets with a single DI water droplet initially in contact with the sensor. Multiple droplets were successfully actuated to the sensor by applying a  $1 \text{ kHz}$  AC voltage in the range of  $40\text{--}80V_{p-p}$ . Fig. 4 shows a resonant wavelength trace from the measurement. The trace shows negligible change in the resonant wavelength after each droplet was merged with the droplet in contact with the sensor.

b) *Glucose Measurement:* To determine the sensitivity of the PL patterned sensors integrated with the EWD system, a glucose solution was used as the refractive index standard.

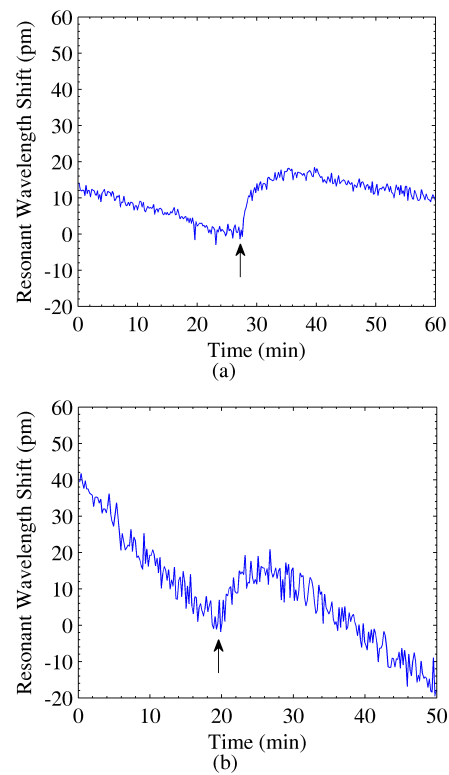


Fig. 5. Sensorgrams for glucose measurements in the electrowetting system. (a) 2% D-glucose droplet merging with a DI  $\text{H}_2\text{O}$  droplet in 20 cSt silicone oil. (b) 2% D-glucose droplet merging with a DI  $\text{H}_2\text{O}$  droplet in 2 cSt silicone oil.

To measure the sensor response to changes in glucose concentration, a droplet of 2% D-glucose was merged with a droplet of DI water already in contact with the sensor.

Two viscosities of silicone oil were tested to assess the impact of the oil on the sensing operation, 20 cSt and 2 cSt. The sensorgrams for each experiment are shown in Fig. 5(a) and Fig. 5(b). For the 20 cSt silicone oil measurement, a resonant wavelength shift of about  $21 \text{ pm}/\%$  was measured, and for the 2 cSt silicone oil measurement, a shift of about  $31 \text{ pm}/\%$  was measured, factoring out the baseline drift. The estimated sensor sensitivity for the 20 cSt and the 2 cSt silicone oil was  $15 \text{ nm/RIU}$  and  $22 \text{ nm/RIU}$ , respectively. These sensitivities were 58% and 85% of the nominal sensitivity, respectively. The 2 cSt silicone oil was the lowest viscosity silicone oil that could be practically utilized in the EWD system, as lower viscosity oils evaporated too rapidly. The observed reduction in sensitivity in the silicone oil medium was most likely due to the presence of a film of oil entrained between the droplet and the sensor. Because the sensitivity of the sensor is proportional to the overlap fraction of the evanescent tail with the sensing region [37], the oil thickness should optimally be much less than the length of the evanescent tail of the guided optical mode propagating in the microresonator ( $\sim 300\text{--}400 \text{ nm}$  [28]). The Q factor for this device was 17,000 for the integrated system glucose measurements [60]. In 2 cSt silicone oil, the EWD integrated FOM was  $0.37 \times 10^6 \text{ nm/RIU}$ , which was comparable to that of the EWD bonded SU-8 microresonator sensor reported by Luan *et al.* [35].

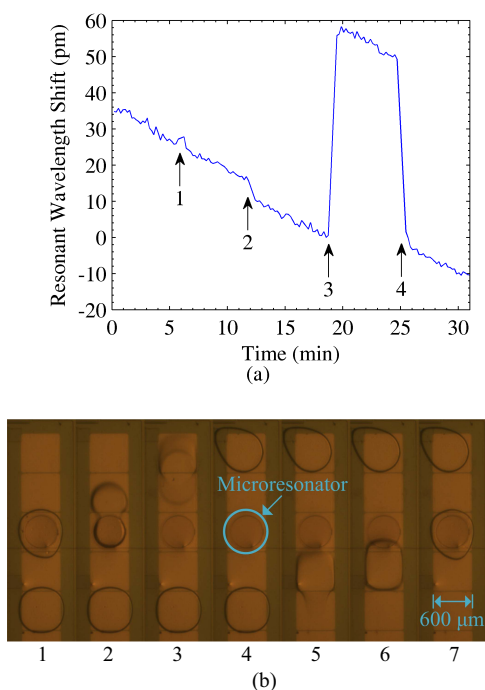


Fig. 6. Droplet swapping experiment data. (a) Sensorgram showing swapping of DI H<sub>2</sub>O with DI H<sub>2</sub>O and with 2% D-glucose and vice-versa in the electrowetting system. 1- DI droplet moved off and then back on. 2- Failed attempt to move DI droplet. 3- DI droplet moved off and glucose droplet moved on. 4- Glucose droplet moved off and DI H<sub>2</sub>O droplet moved on. (b) Image sequence showing the swap of a single DI H<sub>2</sub>O droplet with a single 2% D-glucose droplet under the microresonator sensor (left-to-right, 1 to 7).

For the EBL patterned sensors, the same integrated EWD test was performed. The sensitivity was measured to be 72 nm/RIU in 2 cSt silicone oil, 80% of the nominal sensitivity, and the Q factor was measured to be 8,400 [56]. This Q and S yielded a FOM of  $0.6 \times 10^6$  nm/RIU, which was nearly a factor of two improvement over the PL patterned sensors. This increase in FOM was due to the increase in sensitivity, which arose from the smaller dimensioned waveguides. The smaller dimensioned waveguides confined the optical field so that there was a larger percentage of the field in the target material (the water droplet).

## 2) Droplet Swapping:

a) *Baseline Test and Glucose Measurement:* Glucose measurement by droplet swapping was evaluated using the PL patterned sensors. First, the baseline variability was evaluated by moving a droplet of DI H<sub>2</sub>O in from an electrode to the sensor, and then off of the sensor to an adjacent electrode, then moving it back onto the sensor again. The wavelength trace from this experiment, shown in Fig. 6(a), indicates that the baseline shift was negligible. Only a limited number of swaps onto and off of the sensor were possible. Droplet actuation may have become inhibited after several actuation cycles by a mechanism related to charge build-up, aggravated by the removal of the ITO conductive ground plane in the sensor area, or by droplet adhesion to the SU-8 microresonator.

Following the baseline variability measurements, a swap with a 2% D-glucose droplet was successfully executed, followed by another swap with a DI water droplet. Fig. 6(b)

shows the image sequence for the droplet motion during a swap of the DI water droplet with a 2% D-glucose droplet. The wavelength shift produced by swapping droplets was about 30 pm/% for the first swap and about 26 pm/% for the second swap. Using the average of these two measured shifts, the sensitivity was estimated to be 20 nm/RIU, 77% of the nominal value. This value agrees well with the value measured by the droplet merging method.

## IV. CONCLUSION

A microresonator sensor embedded in the top plate of an electrowetting-on-dielectric microfluidic system was reported for the first time. This integrated system was the first demonstration of a microresonator integrated into an EWD system with full droplet movement capability. The results from this research demonstrate that a microresonator can sense index of refraction variation for fluids when the droplets are in an oil medium. Quantitative measurements of the reduction in sensor sensitivity with different silicone oil viscosities demonstrate the effect of the viscosity of the medium on the sensor sensitivity. The fluidic operations of droplet merging and droplet swapping on the microresonator sensor were demonstrated, indicating low noise droplet merging and swapping. These results indicate that optical microresonator sensors integrated into EWD microfluidics systems have excellent potential for the realization of POC systems.

## ACKNOWLEDGMENT

The authors would like to thank R. Evans, B. Hsu, Y. Lin, and A. Madison for their assistance with the electrowetting system design, for their generous donation of materials, and for assistance with testing the EWD microfluidics.

## REFERENCES

- [1] L. Gervais, N. de Rooij, and E. Delamarque, "Microfluidic chips for point-of-care immunodiagnosics," *Adv. Mater.*, vol. 23, no. 24, pp. H151–H176, Jun. 2011.
- [2] D. Mark, S. Haerberle, G. Roth, F. von Stetten, and R. Zengerle, "Microfluidic lab-on-a-chip platforms: Requirements, characteristics and applications," *Chem. Soc. Rev.*, vol. 39, no. 3, pp. 1153–1182, Jan. 2010.
- [3] A. L. Washburn and R. C. Bailey, "Photonics-on-a-chip: Recent advances in integrated waveguides as enabling detection elements for real-world, lab-on-a-chip biosensing applications," *Analyst*, vol. 136, no. 2, pp. 227–236, Jan. 2011.
- [4] E. G. Hvastkovs and D. A. Buttry, "Recent advances in electrochemical DNA hybridization sensors," *Analyst*, vol. 135, no. 8, pp. 1817–1829, Aug. 2010.
- [5] J. L. Arlett, E. B. Myers, and M. L. Roukes, "Comparative advantages of mechanical biosensors," *Nature Nanotechnol.*, vol. 6, no. 4, pp. 203–215, Mar. 2011.
- [6] S. Y. Teh, R. Lin, L. H. Hung, and A. P. Lee, "Droplet microfluidics," *Lab Chip*, vol. 8, no. 2, pp. 198–220, 2008.
- [7] Z. Hua, J. L. Rouse, A. E. Eckhardt, V. Srinivasan, V. K. Pamula, W. A. Schell, J. L. Benton, T. G. Mitchell, and M. G. Pollack, "Multiplexed real-time polymerase chain reaction on a digital microfluidic platform," *Anal. Chem.*, vol. 82, no. 6, pp. 2310–2316, Feb. 2010.
- [8] R. Sista, Z. S. Hua, P. Thwar, A. Sudarsan, V. Srinivasan, A. Eckhardt, M. Pollack, and V. Pamula, "Development of a digital microfluidic platform for point of care testing," *Lab Chip*, vol. 8, no. 12, pp. 2091–2104, 2008.
- [9] M. G. Pollack, V. K. Pamula, V. Srinivasan, and A. E. Eckhardt, "Applications of electrowetting-based digital microfluidics in clinical diagnostics," *Expert Rev. Molecular Diagn.*, vol. 11, no. 4, pp. 393–407, May 2011.

- [10] J. Zeng and T. Korsmeyer, "Principles of droplet electrohydrodynamics for lab-on-a-chip," *Lab Chip*, vol. 4, no. 4, pp. 265–277, 2004.
- [11] U. Lehmann, S. Hadjidj, V. K. Parashar, C. Vandevyver, A. Rida, and M. A. M. Gijs, "Two-dimensional magnetic manipulation of microdroplets on a chip as a platform for bioanalytical applications," *Sens. Actuators B, Chem.*, vol. 117, no. 2, pp. 457–463, 2006.
- [12] Y. Bourquin, J. Reboud, R. Wilson, and J. M. Cooper, "Tuneable surface acoustic waves for fluid and particle manipulations on disposable chips," *Lab Chip*, vol. 10, no. 15, pp. 1898–1901, Aug. 2010.
- [13] M. K. Tan, L. Y. Yeo, and J. R. Friend, "Rapid fluid flow and mixing induced in microchannels using surface acoustic waves," *Europhys. Lett.*, vol. 87, no. 4, p. 6, Aug. 2009.
- [14] Y. Q. Fu, L. Garcia-Gancedo, H. F. Pang, S. Porro, Y. W. Gu, J. K. Luo, X. T. Zu, F. Placido, J. I. B. Wilson, A. J. Flewitt, and W. I. Milne, "Microfluidics based on ZnO/nanocrystalline diamond surface acoustic wave devices," *Biomicrofluidics*, vol. 6, no. 2, pp. 024105-1–024105-11, Jun. 2012.
- [15] V. Srinivasan, V. K. Pamula, and R. B. Fair, "An integrated digital microfluidic lab-on-a-chip for clinical diagnostics on human physiological fluids," *Lab Chip*, vol. 4, no. 4, pp. 310–315, 2004.
- [16] J. Song, R. Evans, Y. Y. Lin, B. N. Hsu, and R. Fair, "A scaling model for electrowetting-on-dielectric microfluidic actuators," *Microfluidics Nanofluidics*, vol. 7, no. 1, pp. 75–89, Jul. 2009.
- [17] R. B. Fair, "Digital microfluidics: Is a true lab-on-a-chip possible?" *Microfluidics Nanofluidics*, vol. 3, no. 3, pp. 245–281, Jun. 2007.
- [18] A. A. Darhuber and S. M. Troian, "Principles of microfluidic actuation by modulation of surface stresses," *Annu. Rev. Fluid Mech.*, vol. 37, no. 1, pp. 425–455, 2005.
- [19] R. McKendry, J. Y. Zhang, Y. Arntz, T. Strunz, M. Hegner, H. P. Lang, M. K. Baller, U. Certa, E. Meyer, H. J. Guntherodt, and C. Gerber, "Multiple label-free biodection and quantitative DNA-binding assays on a nanomechanical cantilever array," *Proc. Nat. Acad. Sci. United States Amer.*, vol. 99, no. 15, pp. 9783–9788, Jul. 2002.
- [20] E. Ouellet, C. Lausted, T. Lin, C. W. T. Yang, L. Hood, and E. T. Lagally, "Parallel microfluidic surface plasmon resonance imaging arrays," *Lab Chip*, vol. 10, no. 5, pp. 581–588, 2010.
- [21] G. D. Kim, G. S. Son, H. S. Lee, K. D. Kim, and S. S. Lee, "Integrated photonic glucose biosensor using a vertically coupled microring resonator in polymers," *Opt. Commun.*, vol. 281, no. 18, pp. 4644–4647, Sep. 2008.
- [22] J. J. Hu, N. Carlie, N. N. Feng, L. Petit, A. Agarwal, K. Richardson, and L. Kimerling, "Planar waveguide-coupled, high-index-contrast, high-Q resonators in chalcogenide glass for sensing," *Opt. Lett.*, vol. 33, no. 21, pp. 2500–2502, Nov. 2008.
- [23] J. Cooper, N. Yazvenko, K. Peyvan, K. Maurer, C. R. Taitt, W. Lyon, and D. L. Danley, "Targeted deposition of antibodies on a multiplex CMOS microarray and optimization of a sensitive immunoassay using electrochemical detection," *PLoS One*, vol. 5, no. 3, p. e9781, Mar. 2010.
- [24] T. Uno, H. Tabata, and T. Kawai, "Peptide-nucleic acid-modified ion-sensitive field-effect transistor-based biosensor for direct detection of DNA hybridization," *Anal. Chem.*, vol. 79, no. 1, pp. 52–59, Jan. 2007.
- [25] A. M. Armani, R. P. Kulkarni, S. E. Fraser, R. C. Flagan, and K. J. Vahala, "Label-free, single-molecule detection with optical microcavities," *Science*, vol. 317, no. 5839, pp. 783–787, Aug. 2007.
- [26] J. G. Zhu, S. K. Ozdemir, Y. F. Xiao, L. Li, L. N. He, D. R. Chen, and L. Yang, "On-chip single nanoparticle detection and sizing by mode splitting in an ultrahigh-Q microresonator," *Nature Photon.*, vol. 4, no. 1, pp. 46–49, Jan. 2010.
- [27] N. Jokerst, M. Royal, S. Palit, L. Luan, S. Dhar, and T. Tyler, "Chip scale integrated microresonator sensing systems," *J. Biophoton.*, vol. 2, no. 4, pp. 212–226, Apr. 2009.
- [28] A. Yalcin, K. C. Popat, J. C. Aldridge, T. A. Desai, J. Hryniewicz, N. Chbouki, B. E. Little, O. King, V. Van, S. Chu, D. Gill, M. Anthes-Washburn, and M. S. Unlu, "Optical sensing of biomolecules using microring resonators," *IEEE J. Sel. Topics Quantum Electron.*, vol. 12, no. 1, pp. 148–155, Jan./Feb. 2006.
- [29] M. Iqbal, M. A. Gleeson, B. Spaugh, F. Tybor, W. G. Gunn, M. Hochberg, T. Baehr-Jones, R. C. Bailey, and L. C. Gunn, "Label-free biosensor arrays based on silicon ring resonators and high-speed optical scanning instrumentation," *IEEE J. Sel. Topics Quantum Electron.*, vol. 16, no. 3, pp. 654–661, May/June. 2010.
- [30] C. Y. Chao, W. Fung, and L. J. Guo, "Polymer microring resonators for biochemical sensing applications," *IEEE J. Sel. Topics Quantum Electron.*, vol. 12, no. 1, pp. 134–142, Jan./Feb. 2006.
- [31] S. Y. Cho and N. M. Jokerst, "A polymer microdisk photonic sensor integrated onto silicon," *IEEE Photon. Technol. Lett.*, vol. 18, no. 20, pp. 2096–2098, Oct. 2006.
- [32] M. S. Kwon and W. H. Steier, "Microring-resonator-based sensor measuring both the concentration and temperature of a solution," *Opt. Exp.*, vol. 16, no. 13, pp. 9372–9377, Jun. 2008.
- [33] C. Delezoide, M. Salsac, J. Lautru, H. Leh, C. Nogues, J. Zyss, M. Buckle, I. Ledoux-Rak, and N. Chi Thanh, "Vertically coupled polymer microracetrack resonators for label-free biochemical sensors," *IEEE Photon. Technol. Lett.*, vol. 24, no. 4, pp. 270–272, Feb. 2012.
- [34] L. Luan, R. D. Evans, D. Schwinn, R. B. Fair, and N. M. Jokerst, "Chip scale integration of optical microresonator sensors with digital microfluidics systems," in *Proc. 21st Annu. Meet. IEEE/LEOS*, Nov. 2008, pp. 259–260.
- [35] L. Luan, M. Royal, R. Evans, R. Fair, and N. Jokerst, "Chip scale optical microresonator sensors integrated with embedded thin film photodetectors on electrowetting digital microfluidics platforms," *IEEE Sensors J.*, vol. 12, no. 6, pp. 1794–1800, Dec. 2011.
- [36] C. Y. Chao and L. J. Guo, "Design and optimization of microring resonators in biochemical sensing applications," *J. Lightw. Technol.*, vol. 24, no. 3, pp. 1395–1402, Mar. 2006.
- [37] J. J. Hu, X. C. Sun, A. Agarwal, and L. C. Kimerling, "Design guidelines for optical resonator biochemical sensors," *J. Opt. Soc. Amer. B, Opt. Phys.*, vol. 26, no. 5, pp. 1032–1041, May 2009.
- [38] P. Rabiei, W. H. Steier, C. Zhang, and L. R. Dalton, "Polymer microring filters and modulators," *J. Lightw. Technol.*, vol. 20, no. 11, pp. 1968–1975, Nov. 2002.
- [39] V. Van, P. P. Absil, J. V. Hryniewicz, and P. T. Ho, "Propagation loss in single-mode GaAs-AlGaAs microring resonators: Measurement and model," *J. Lightw. Technol.*, vol. 19, no. 11, pp. 1734–1739, Nov. 2001.
- [40] C. A. Barrios, "Analysis and modeling of a silicon nitride slot-waveguide microring resonator biochemical sensor," *Proc. SPIE*, vol. 7356, p. 735605, Apr. 2009.
- [41] C. A. Barrios, K. B. Gylfason, B. Sanchez, A. Griol, H. Sohlstrom, M. Hologado, and R. Casquel, "Slot-waveguide biochemical sensor," *Opt. Lett.*, vol. 32, no. 21, pp. 3080–3082, Nov. 2007.
- [42] K. Tiefenthaler and W. Lukosz, "Sensitivity of grating couplers as integrated-optical chemical sensors," *J. Opt. Soc. Amer. B, Opt. Phys.*, vol. 6, no. 2, pp. 209–220, Feb. 1989.
- [43] S. Arnold, M. Khoshshima, I. Teraoka, S. Holler, and F. Vollmer, "Shift of whispering-gallery modes in microspheres by protein adsorption," *Opt. Lett.*, vol. 28, no. 4, pp. 272–274, Feb. 2003.
- [44] D. K. Armani, T. J. Kippenberg, S. M. Spillane, and K. J. Vahala, "Ultra-high-Q toroid microcavity on a chip," *Nature*, vol. 421, no. 6926, pp. 925–928, Feb. 2003.
- [45] D. X. Xu, A. Densmore, A. Delage, P. Waldron, R. McKinnon, S. Janz, J. Lapointe, G. Lopinski, T. Mischki, E. Post, P. Cheben, and J. H. Schmid, "Folded cavity SOI microring sensors for high sensitivity and real time measurement of biomolecular binding," *Opt. Exp.*, vol. 16, no. 19, pp. 15137–15148, Sep. 2008.
- [46] H. Ma, A. K. Y. Jen, and L. R. Dalton, "Polymer-based optical waveguides: Materials, processing, and devices," *Adv. Mater.*, vol. 14, no. 19, pp. 1339–1365, Oct. 2002.
- [47] W. Bogaerts, P. De Heyn, T. Van Vaerenbergh, K. De Vos, S. K. Selvaraja, T. Claes, P. Dumon, P. Bienstman, D. Van Thourhout, and R. Baets, "Silicon microring resonators," *Laser Photon. Rev.*, vol. 6, no. 1, pp. 47–73, Jan. 2011.
- [48] B. E. Little, S. T. Chu, W. Pan, D. Ripin, T. Kaneko, Y. Kokubun, and E. Ippen, "Vertically coupled glass microring resonator channel dropping filters," *IEEE Photon. Technol. Lett.*, vol. 11, no. 2, pp. 215–217, Feb. 1999.
- [49] F. D. Egitto and L. J. Matienzo, "Plasma modification of polymer surfaces for adhesion improvement," *IBM J. Res. Develop.*, vol. 38, no. 4, pp. 423–439, Jul. 1994.
- [50] S. A. Makohliso, L. Giovangrandi, D. Laconard, H. J. Mathieu, M. Ilegems, and P. Aebischer, "Application of Teflon-AF thin films for bio-patterning of neural cell adhesion," *Biosens. Bioelectron.*, vol. 13, no. 11, pp. 1227–1235, Nov. 1998.
- [51] T. Gerfin and M. Gratzel, "Optical properties of tin-doped indium oxide determined by spectroscopic ellipsometry," *J. Appl. Phys.*, vol. 79, no. 3, pp. 1722–1729, Feb. 1996.
- [52] *SU-8 3000 Permanent Epoxy Negative Photoresist*, Microchem, Inc., Santa Clara, CA, USA, Oct. 2011.
- [53] *Parylene Properties*, Specialty Coating Syst., Inc., Indianapolis, IN, USA, Jan. 2012.
- [54] *CYTOP Data*, Asahi Glass Co., Ltd., Tokyo, Japan, Jul. 2009.
- [55] *SU-8 2000 Permanent Epoxy Negative Photoresist*, Microchem, Inc., Santa Clara, CA, USA, Oct. 2011.

- [56] M. Royal, N. Jokerst, and R. Fair, "Integrated sample preparation and sensing: Polymer microresonator sensors embedded in digital electrowetting microfluidic systems," *IEEE Photon. J.*, vol. 4, no. 6, pp. 2126–2135, Dec. 2012.
- [57] M. G. Pollack, R. B. Fair, and A. D. Shenderov, "Electrowetting-based actuation of liquid droplets for microfluidic applications," *Appl. Phys. Lett.*, vol. 77, no. 11, pp. 1725–1726, Jul. 2000.
- [58] Y. Liu, P. Hering, and M. O. Scully, "An integrated optical sensor for measuring glucose concentration," *Appl. Phys. B, Lasers Opt.*, vol. 54, no. 1, pp. 18–23, Jan. 1992.
- [59] G. C. Hill, R. Melamud, F. E. Declercq, A. A. Davenport, I. H. Chan, P. G. Hartwell, and B. L. Pruitt, "SU-8 MEMS Fabry–Perot pressure sensor," *Sens. Actuators A, Phys.*, vol. 138, no. 1, pp. 52–62, Jul. 2007.
- [60] M. W. Royal, R. B. Fair, and N. M. Jokerst, "Integrated sample preparation and sensing: Microresonator optical sensors embedded in digital electrowetting microfluidics systems," in *Proc. IEEE SENSORS*, Oct. 2011, pp. 2050–2053.



**Matthew W. Royal** received the Ph.D. and M.S. degrees in electrical engineering from Duke University, Durham, NC, USA, in 2012 and 2008, respectively, and the B.S. degree in engineering science from The Pennsylvania State University, State College, PA, USA, in 2006.

He is currently a Post-Doctoral Associate with Prof. Fair's Digital Microfluidics Group, Duke University.

Dr. Royal was supported by the National Defense Science and Engineering Graduate Fellowship for research and development of microresonator biosensors from 2007 to 2010.



**Nan M. Jokerst** (F'03) received the Ph.D. degree in electrical engineering from the University of Southern California, Los Angeles, CA, USA, in 1989. She is the J. A. Jones Professor of electrical and computer engineering with Duke University, Durham, NC, USA.

She has published more than 250 papers in refereed journals and conference proceedings, three book chapters, and has four patents awarded in the areas of chip-scale integrated systems, sensors, integrated photonics, optical interconnections, and

metamaterials.

Prof. Jokerst received the IEEE Education Society/Hewlett Packard Harriet B. Rigas Medal in 2002 and the IEEE Millennium Medal in 2000. She is a fellow of the Optical Society of America in 2000. She is a DuPont Young Faculty Awardee and the National Science Foundation Presidential Young Investigator, and has won a Newport Research Award, three teaching awards, and was a Hewlett Packard Fellow. She has organized and served on numerous conference committees, and served on the Board of Directors of the Optical Society of America as the Chair of the Engineering Council, on the IEEE Lasers and Electro-Optic Society Board of Governors as an Elected Member, and as the Vice President of Conferences and the Vice President of Technical Affairs. She has served as the elected Chair, Vice Chair, Secretary, and Treasurer of the Atlanta IEEE Section.



**Richard B. Fair** (S'63–M'75–SM'75–F'90) received the Ph.D. degree from Duke University, Durham, NC, USA, in 1969.

He was with Bell Laboratory, Murray Hill, NJ, USA, on semiconductor devices and integrated-circuit technology. He returned to North Carolina in 1981 and spent 13 years as a Vice President of Microelectronics Center of North Carolina, having responsibilities in chip design, computer-aided design, packaging, process technology, and microelectromechanical systems (MEMS). He is

currently a Professor of electrical and computer engineering with Duke University. He has published over 150 papers in refereed journals and conference proceedings, written ten book chapters, edited nine books or conference proceedings, and given over 120 invited talks, mostly in the area of semiconductor devices or the fabrication thereof. His current research interests include bio-MEMS and digital microfluidic chips. His research group first demonstrated microdroplet transport over electrode arrays based on electrowetting actuation.

Dr. Fair is a fellow of the Electrochemical Society, past Editor-in-Chief of the *Proceedings of the IEEE*, and he has served as an Associate Editor of the IEEE TRANSACTIONS ON ELECTRON DEVICES. He is a recipient of the IEEE Third Millennium Medal in 2000 and the 2003 Solid State Science and Technology Prize and Medal from the Electrochemical Society, Paris, France.